INTERNATIONAL JOURNAL OF CLIMATOLOGY
Int. J. Climatol. **34**: 3336–3347 (2014)
Published online 30 December 2013 in Wiley Online Library
(wileyonlinelibrary.com) DOI: 10.1002/joc.3911

RMetS
Royal Meteorological Society

Tree-ring δ^{18}O evidence for the drought history of eastern Tianshan Mountains, northwest China since 1700 AD

Guobao Xu,[a,b] Xiaohong Liu,[a*] Dahe Qin,[a] Tuo Chen,[a] Wenzhi Wang,[a,b] Guoju Wu,[a,b] Weizhen Sun,[a] Wenling An[a,b] and Xiaomin Zeng[a,b]

[a] *State Key Laboratory of Cryospheric Sciences, Cold and Arid Regions Environmental and Engineering Research Institute, Lanzhou, China*
[b] *University of Chinese Academy of Sciences, Beijing, China*

ABSTRACT: We developed an annual tree-ring δ^{18}O chronology from *Larix sibirica* in the eastern Tianshan Mountains of northwestern China. Climatic response revealed that tree-ring δ^{18}O was significantly positively correlated with the mean and maximum July–August temperatures, whereas the July precipitation and relative humidity were significantly negatively correlated with tree-ring δ^{18}O. The self-calibrating Palmer drought severity index (sc_PDSI) in July–August was significantly correlated with the tree-ring δ^{18}O, which reflects the comprehensive effects of the three parameters on tree-ring δ^{18}O fractionation. We established a robust reconstruction of July–August sc_PDSI that accounted for 38.4% of the total variance of sc_PDSI from 1959 to 2008. The sc_PDSI reconstruction yields new insights on past drought that were not previously realized in other PDSI reconstructions (e.g. Monsoon Asia Drought Atlas) from the region. The reconstruction revealed several wet and dry periods but no trend towards a wetter climate in the eastern Tianshan Mountains during the last two decades. It also detected synergistic effects of the North Atlantic Oscillation and the El Niño-Southern Oscillation on regional moisture conditions as a result of teleconnections between tropical oceans and mid-latitude circulation patterns.

KEY WORDS tree-ring δ^{18}O; self-calibrating PDSI; drought reconstruction; northwestern China; NAO; ENSO

Received 19 April 2013; Revised 24 November 2013; Accepted 28 November 2013

1. Introduction

In recent decades, drought events appear to be increasing in intensity and frequency in response to climate warming over Asia (Easterling *et al.*, 2000), especially in semi-arid to arid regions such as northern China (Ma and Fu, 2006). It is thus important to understand drought patterns over long-time scale as well as the mechanisms responsible for these patterns. Understanding climate variability and long-term trends in moisture variability for periods before instrumental data is available is vital to regional hydrological management and agriculture.

The Palmer drought severity index (PDSI) is often used as a drought metric because it can assess the severity of drought conditions (Palmer, 1965). PDSI has been used to study the drought variability over the Asia (Cook *et al.*, 2010), northern China (Fang *et al.*, 2012) and the central Tianshan Mountains of northwestern China (Li *et al.*, 2006) in combination with tree-ring width. One of the most common problems of PDSI is that PDSI values are not comparable between diverse climatological regions (Wells *et al.*, 2004). Efforts to address major problems of PDSI have led to a new variant of the PDSI, the self-calibrating PDSI (sc_PDSI) (Wells *et al.*, 2004), which has been used to assess the drought (Dai, 2011). Tree-ring oxygen isotope ratio (δ^{18}O) series have an advantage for PDSI reconstruction in that the physiological controls on the isotopic composition are well understood and relatively simple compared to many factors that control tree-ring growth (Roden and Ehleringer, 2000; Roden *et al.*, 2000; Waterhouse *et al.*, 2002; McCarroll and Loader, 2004; Treydte *et al.*, 2006; Sano *et al.*, 2012a). Tree-ring δ^{18}O is primarily controlled by δ^{18}O of source water and relative humidity (e.g. Roden *et al.*, 2000, Robertson *et al.*, 2001; McCarroll and Loader, 2004), both of which are directly related to the regional moisture conditions (wet–dry conditions). Tree-ring δ^{18}O has been used successfully to reconstruct PDSI, which was used to assess aridity change and to detect possible linkage with atmospheric circulations (Xu *et al.*, 2011; Sano *et al.*, 2012a, 2012b). It has also been reported that tree-ring δ^{18}O was much more sensitive to PDSI than tree-ring width (Xu *et al.*, 2011). Another advantage of the tree-ring δ^{18}O is that this parameter is weak or little affected by the tree's age (Saurer *et al.*, 2002; McCarroll and Loader, 2004; Anchukaitis and Evans, 2010; Daux *et al.*, 2011; Shi *et al.*, 2011; Young *et al.*, 2011), except for a few studies (Treydte *et al.*, 2006; Esper *et al.*, 2010).

Herein, we established a 309-year annual resolution tree-ring δ^{18}O chronology using Siberian larch (*Larix*

* Correspondence to: X. Liu, State Key Laboratory of Cryospheric Sciences, Cold and Arid Regions Environmental and Engineering Research Institute, Chinese Academy of Sciences, Donggang West Road No. 320, Lanzhou 730000, China. E-mail: liuxh@lzb.ac.cn

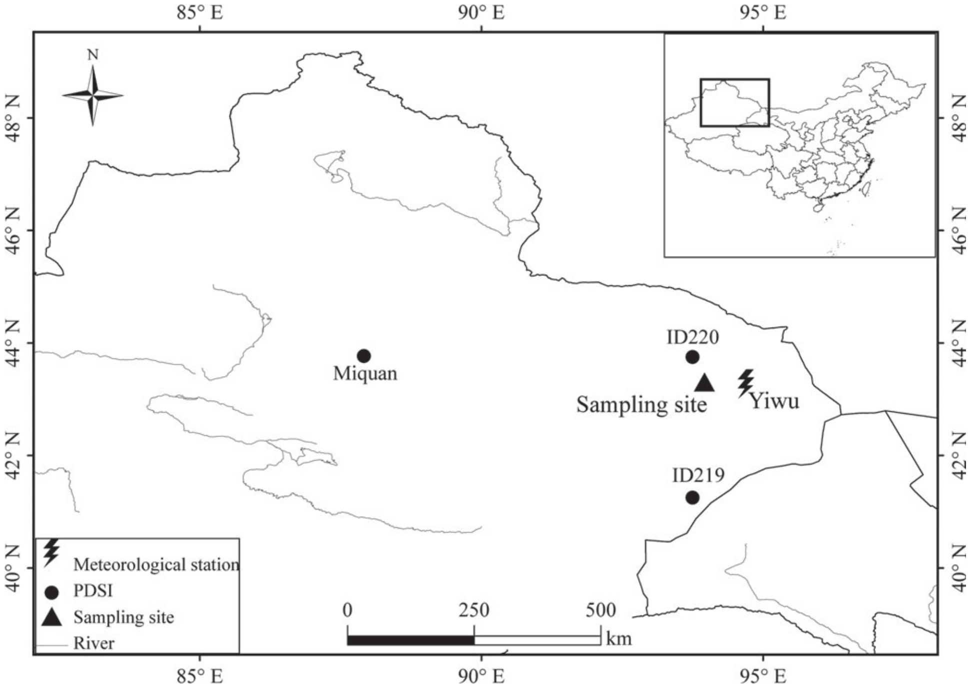

Figure 1. Map of location of the sampling site and nearby PDSI data and meteorological stations. ID 220 (43.75°N, 93.75°), location of sc_PDSI data from 1948 to 2008 (Dai, 2011) used in this study. ID 220 and ID 219 (41.25°N, 93.75°E), locations from the MADA dataset (Cook *et al.*, 2010).

sibirica Ldb) trees from the eastern Tianshan Mountains, an important arid inland area of northwestern China. The primary aim of the study was to detect the climatic implication of the tree-ring δ^{18}O series in this arid area. Completion of this objective revealed a close association with sc_PDSI, and this understanding was used to explore potential sc_PDSI reconstruction and to understand the history and possible driving forces which are responsible for the variability in drought intensity in the region.

2. Materials and methods

2.1. Study site and wood samples

The study area is located in the Hami region of the eastern Tianshan Mountains (Figure 1). Owing to its location within the interior of the Eurasian continent, little moisture reaches this region from the Pacific Ocean, Arctic Ocean and Indian Ocean. The central Asia westerly circulation has been shown to dominate the study area's climate in all seasons based on precipitation isotopic data and climatic reanalysis data (Dai *et al.*, 2006; Tian *et al.*, 2007; Li *et al.*, 2008; Liu *et al.*, 2009b; Rashed *et al.*, 2010). The virgin forest in the areas of the Tianshan Mountains is found at elevations ranging from 1800 to 2750 m a.s.l., and the dominant tree species are Siberian larch and Tianshan spruce (*Picea schrenkiana*). The Siberian larch with resistance to both cold and drought is distributed at higher elevations than the spruce. The Siberian larch forms surface root systems as well as adventitious roots; therefore, it has a shallow root system (Abaimov, 2010). The larch forms pure stands with a crown cover of 10–15% and a distance of about 10 m between trees at the sampling site (43.31°N, 93.96°E; Figure 1). The growing season for larch is from May to September in the study area (Zhou *et al.*, 1989). We collected 43 tree-ring cores (two cores per tree) from old-growth larch growing at altitudes ranging from 2710 to 2740 m a.s.l. at the upper treeline using a 12-mm diameter increment borer (Haglöf, Mora, Sweden) at breast height (about 1.3 m above the ground) in September 2008.

All cores were air-dried and then polished using progressively finer grades of sandpaper. After the cellular structure had been clearly revealed, all cores were visually cross-dated using a standard methodology (Stokes and Smiley, 1968), resulting in the absolute assignment of calendar years to every growth year. We measured all cross-dated growth rings to a precision of 0.01 mm using a sliding stage micrometer (LINTAB 6; Rinntech, Heidelberg, Germany) interfaced with a computer using the time series analysis and presentation features of the device's dendrochronological software (Rinn, 2003). We confirmed the cross-dating using the COFECHA software (Holmes, 1983) (http://www.ncdc.noaa.gov/paleo/treering/cofecha/cofecha.html).

2.2. Tree-ring isotope analysis

We selected 13 cores (one core per tree) from trees with homogeneous growth patterns to obtain enough wood material. Many rings were narrow or had indistinct latewood, so we used the whole wood from each year for the isotopic analyses (Liu *et al.*, 2009a). We then pooled the contemporaneous annual wood samples prior

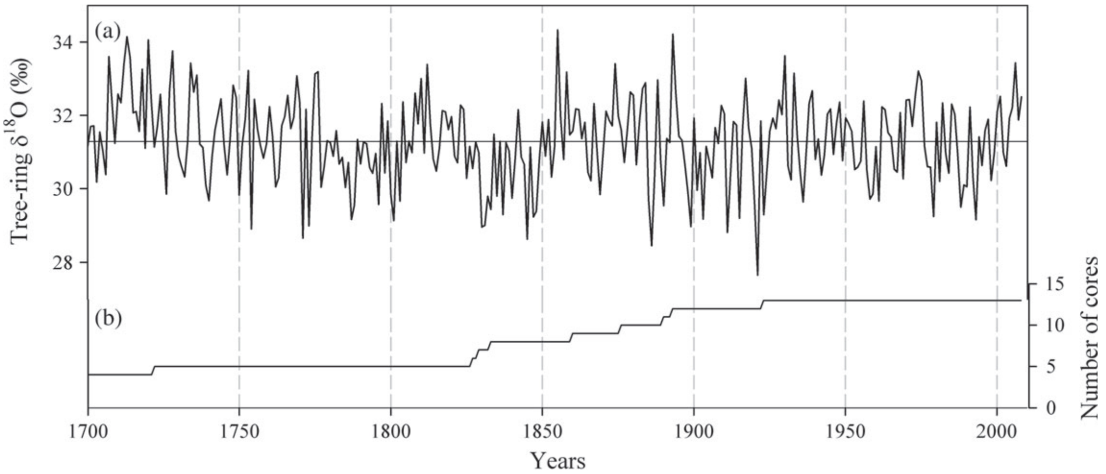

Figure 2. (a) Tree-ring δ^{18}O series for the entire period covered by our data and (b) the number of cores available during each period for the isotopic analyses.

to α-cellulose extraction without considering the different contribution of single trees (Leavitt, 2008; Liu *et al.*, 2009a; Shi *et al.*, 2011; Szymczak *et al.*, 2012), and discarded the initial 30 years of every core to negate the potential for juvenile effects (Szymczak *et al.*, 2012). We first milled the pooled annual samples ($< 80\,\mu$m), and then extracted α-cellulose using methods of Loader *et al.* (1997) and Liu *et al.* (2010). To better homogenize the cellulose, we used an ultrasound machine (JY92-2D, Scientz Industry, Ningbo, China) to break the cellulose fibres, following the method of Laumer *et al.* (2009).

For the δ^{18}O measurements, we loaded 0.14–0.16 mg of α-cellulose into silver capsules, and determined the isotope ratio (^{18}O/^{16}O) using a High Temperature Conversion Elemental Analyzer coupled to a Finnigan MAT-253 mass spectrometer (Thermo Electron Corporation, Bremen, Germany) at the state key laboratory of cryospheric sciences, Chinese Academy of Sciences. The δ^{18}O analyses were repeated four times for each annual cellulose sample. After excluding the outliers (values more than three times the standard deviation from the mean), we calculated the mean values. We measured the ratio for a benzoic acid working standard with a known δ^{18}O value (IAEA-601, 23.3‰) for every seven measurements to monitor the analytical precision and to calibrate the samples for analytical accuracy. We also used a cellulose standard (IAEA-C_3, 32.2‰) and commercial cellulose (Fluka Analytical, Sigma-Aldrich, Buchs, Germany, 28.2‰) to calibrate the tree-ring δ^{18}O measurements. Although the cellulose standards were not identical treatment to α-cellulose samples procedure as proposed by Porter and Middlestead (2012), the δ^{18}O value has acceptable reproducibility for the benzoic acid ($\sigma < 0.18$‰, $n = 120$) and cellulose standards ($\sigma < 0.17$‰, $n = 130$ for IAEA-C3; $\sigma < 0.13$‰, $n = 320$ for commercial cellulose) for this project. The mean analytical precision value of 0.34‰ (2σ) for δ^{18}O is acceptable. The final δ^{18}O isotope chronology covered the period from 1700 to 2008 with more than four trees (Figure 2), which is sufficient to achieve an acceptable result of site δ^{18}O chronology as suggested by some tree-ring isotope studies (Treydte *et al.*, 2006; Leavitt, 2010; Shi *et al.*, 2011, Porter *et al.*, 2013).

2.3. Meteorological data

To determine the response of the tree-ring oxygen to climate, we obtained climatic records from the Yiwu meteorological station (43.27°N, 94.7°E, 1729.5 m a.s.l.; Figure 1) which is the nearest station (about 40 km) to the tree sampling site. The climatic variables included the monthly maximum, minimum and mean temperatures, and the monthly precipitation and mean monthly relative humidity. All of the climatic data covered the period from 1959 to 2008. We also compared a sc_PDSI dataset (43.75°, 93.75°) which spanned from 1948 to 2008 and was extracted from a global sc_PDSI dataset (Dai *et al.*, 2004; Dai, 2011). It should be noted that the quality of the sc_PDSI data for western China degrades before the 1950s, because most of the meteorological records in our study area are available after the late 1950s. We only used the sc_PDSI during the common period (from 1959 to 2008) with the meteorological records to calibrate the tree-ring δ^{18}O chronology. The sc_PDSI data from 1948 to 1958, interpolated using nearby meteorological records (Dai, 2011), are used for verification.

The North Atlantic Oscillation (NAO) index represents the strength of the westerly circulation (Hurrell *et al.*, 2001; Li and Wang, 2003; Pinto and Raible, 2012). A new NAO index was recently defined based on the differences between normalized sea-level pressure averaged over longitudes 80°W–30°W (Li and Wang, 2003), using data from 1873 to the present. The new index has a high signal-to-noise ratio, and does a good job of describing the seasonal migration of the NAO's action centers (Li and Wang, 2003). Therefore, we adopted this NAO index to detect the influence of the westerly circulation on the region climate. The El Niño-Southern Oscillation (ENSO) has global teleconnections that influence climate over long distance (Yeh *et al.*, 2009), and influences the drought frequency and severity at mid-latitudes (Hoerling and Kumar, 2003) such as those in central and south-western Asia (Barlow *et al.*, 2002). We therefore also used the Niño 3.4 index from 1856 to 2008 (Kaplan *et al.*, 1998) (http://www.cpc.ncep.noaa.gov) to investigate possible linkages with the regional climate of the study area.

2.4. Statistical and transfer function

To investigate the climate signals in tree-ring isotope series, we calculate its Pearson correlations with climate data. We applied bootstrap resampling methods (Wigley *et al.*, 1984; Davison and Hinkley, 1997) to verify the reliability and stability of these correlations. The window for the response of tree-ring δ^{18}O to climate spanned the period from August of the prior year to September of the current year. We estimated a transfer function by means of linear regression using the sc_PDSI in July–August (JA) (which had the strongest correlation with δ^{18}O; see the results for details) as the dependent variable and the tree-ring δ^{18}O as the independent variable. The sc_PDSI data set from 1959 to 2008 was split into two sub-periods for separate calibration (30 year period) and verification (20 year period) of the dendroclimatic model (Fritts, 1976). We also used sc_PDSI data set from 1959 to 2008 and leave-one-out validation method to verify our reconstruction model. The sign test (ST), correlation coefficient (r), coefficient of efficiency (CE) and reduction of error (RE) were used to validate the reconstruction (Cook and Kairiukstis 1990). The spatial correlation between the reconstruction and the gridded University Corporation for Atmospheric Research (UCAR) sc_PDSI (Dai *et al.*, 2004) and standardized precipitation evapotranspiration index (SPEI) (Vicente-Serrano *et al.*, 2010) data was conducted to verify the reconstruction. In order to validate the reconstruction, it was compared with several moisture reconstructions. We also examined the possibility of large-scale climate drivers (i.e. NAO and ENSO) of moisture conditions at decadal and multi-decadal scales using the fast Fourier transform (FFT) filters (Bergland, 1969). To detect the decadal variation of ENSO and NAO and retain the cycle signals from NAO, we adopted a band-pass filter that preserved the signals at scales of 10–60 years.

3. Results and discussions

3.1. Pooled method and tree-ring δ^{18}O chronology

As suggested by Shi *et al.* (2011), the pooled measurement of tree-ring δ^{18}O without regard to mass is consistent with the mean values of several individuals measured separately. Several other researches have documented the similar findings for carbon and oxygen in tree rings (Leavitt, 2008; Kress *et al.*, 2010; Leavitt, 2010; Liñán *et al.*, 2011; Szymczak *et al.*, 2012). Herein, we consider the pooling method without regard to mass to be an acceptable method for producing a reliable δ^{18}O chronology, although we acknowledge its limitations with respect to calculating signal strength and inter-tree variability statistics.

The δ^{18}O in tree rings averaged $31.3 \pm 1.16‰$ (mean $\pm 1\sigma$; Figure 2) during the study period (1700–2008). The mean δ^{18}O value of the tree-ring chronology is in the range of the European tree-ring δ^{18}O network for *Pinus* (from 26.37 to 33.58‰) (Treydte *et al.*, 2007). The standard deviation (1.16) and the variance (1.35) of the series were low and the range of value in the chronology was 6.67‰. The maximum and minimum values occurred in 1855 (34.33‰) and 1921 (27.65‰), respectively.

3.2. Relationship between tree-ring δ^{18}O and climate

Temperatures (maximum and mean), precipitation and relative humidity in various months showed significant correlations with tree-ring δ^{18}O (Figure 3(a) and (b)). The maximum and mean temperatures from May to August were significantly positively correlated with the tree-ring δ^{18}O (Figure 3(a)). The correlation coefficient reached a maximum of 0.47 ($p < 0.01$) and 0.53 ($p < 0.01$), respectively, for mean temperature and maximum temperature in July–August. Significant correlations were also detected between tree-ring δ^{18}O and relative humidity in the previous December, in March, May and July, and precipitation in March and July (Figure 3(b)). Tree-ring δ^{18}O was also significantly negatively correlated with the precipitation ($r = -0.38$, $p < 0.01$) and relative humidity ($r = -0.54$, $p < 0.001$) in July–August. The relative humidity and mean temperature in July–August explained the variations of tree-ring δ^{18}O about 29.5% ($p < 0.001$) and 21.8% ($p < 0.001$), respectively. Significant negative correlations were also detected between the sc_PDSI values from the previous December to the current September and the tree-ring δ^{18}O and the strongest correlations were 0.71 in July ($p < 0.01$) and 0.65 ($p < 0.01$) in July–August.

Tree-ring δ^{18}O was significantly influenced by the relative humidity (Figure 3(b)), and similar results were obtained in previous studies (Roden *et al.*, 2000; Robertson *et al.*, 2001; Waterhouse *et al.*, 2002; Liu *et al.*, 2012). As relative humidity controls evaporative enrichment of the δ^{18}O of leaf water, lower relative humidity causes a higher vapour-pressure gradient between the leaf's interstitial spaces and the ambient atmosphere, resulting in transpiration enrichment in ^{18}O of the δ^{18}O of leaf water (Roden *et al.*, 2000; Sano *et al.*, 2012a). As a result, the tree-ring δ^{18}O models (Roden *et al.*, 2000; Waterhouse *et al.*, 2002; McCarroll and Loader, 2004; Sternberg, 2009) suggest that the variation of the relative humidity will leave its fingerprints in the tree-ring δ^{18}O. Precipitation and relative humidity are also closely associated, which in turn controls the degree of evaporative enrichment of leaf water δ^{18}O (Roden *et al.*, 2000), and therefore controls tree-ring δ^{18}O.

Temperature indirectly influences the tree-ring δ^{18}O by changing the ambient moisture conditions (e.g.

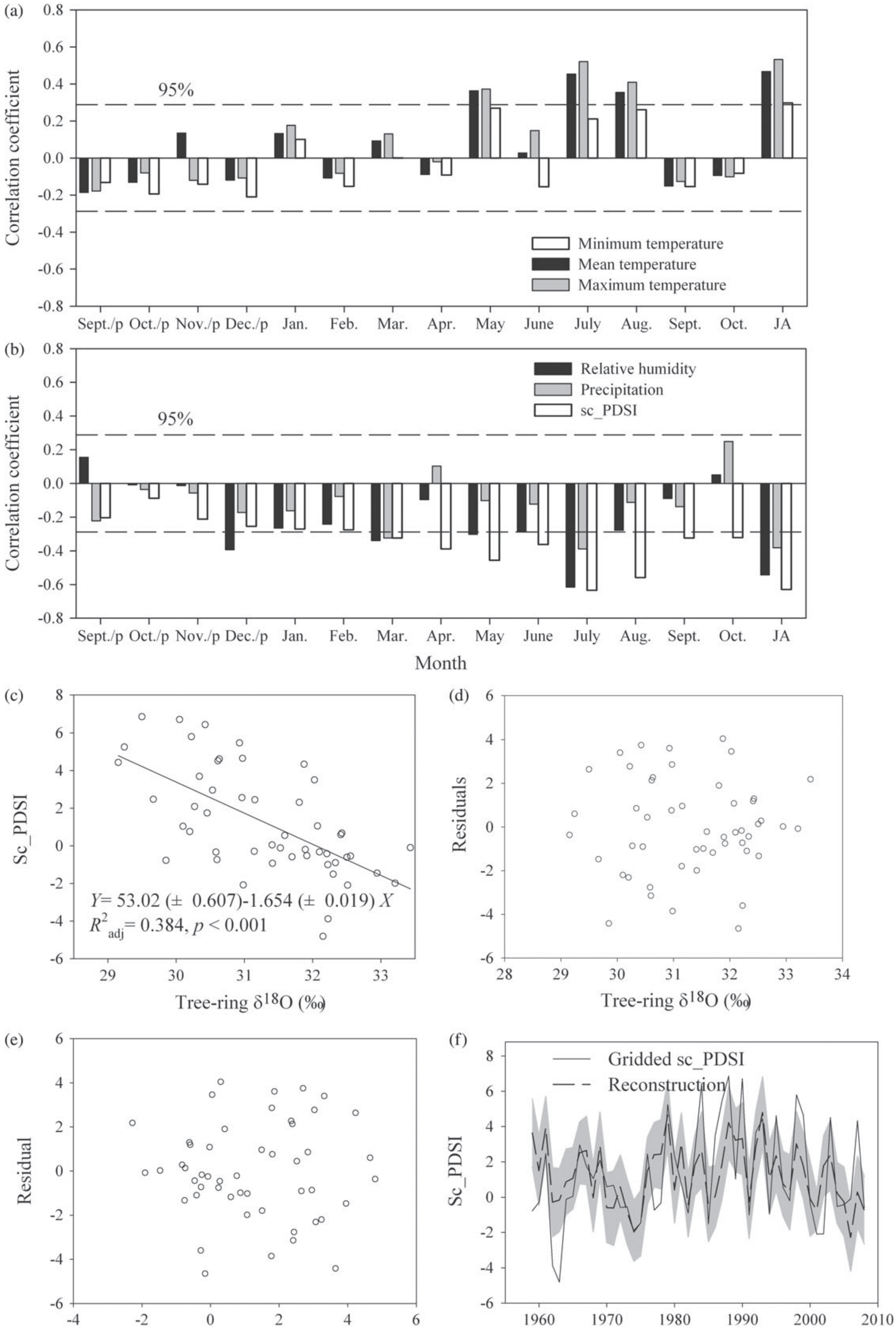

Figure 3. (a, b) The values of Pearson's correlation coefficient between the tree-ring δ^{18}O and climatic variables at the Yiwu station and the sc_PDSI data from 1959 to 2008, (c) the relationship between tree-ring δ^{18}O and corresponding July–August (JA) sc_PDSI data, and (d) the relationship between tree-ring δ^{18}O and the residuals of the linear models in (c), (e) the relationship between reconstructed sc_PDSI from 1959 to 2008 and the residuals of the linear models in (c), and (f) the gridded sc_PDSI data and the reconstructed sc_PDSI time series since 1959. The grey shaded area depicted the uncertainties of reconstruction (see text for details). (a, b) Months followed by '/p' indicate values in the previous year. JA represents the mean value July and August of the current growing season. The dashed lines indicate the 95% confidence intervals. Bars that extend outside the confidence interval represent statistically significant results.

evaporation and transpiration), and this is particularly true in July and August, which are the warmest months in our study area. More specifically, the increasing temperatures increase evaporation of soil water, resulting in a depletion of lighter isotopes from the soil water (Sano *et al.*, 2012a), and this is reflected in the water taken up by trees. In addition, δ^{18}O of the source water is also a primary factor affecting tree-ring δ^{18}O (Roden *et al.*, 2000; McCarroll and Loader, 2004). δ^{18}O of precipitation in the region is controlled by temperature with a positive effect (Liu *et al.*, 2009b) because of the Rayleigh distillation, which is named 'temperature effect' (Dansgaard, 1964). As a shallow root system species, the source water of the larch is primarily from the precipitation. As a consequence, tree-ring δ^{18}O of larch recorded temperature signal to some degree due to the linkage between precipitation δ^{18}O and temperature. Our results indicated that tree-ring δ^{18}O increases with increasing temperature and with decreasing precipitation and relative humidity (Figure 3(a) and (b)), and thus depends strongly on moisture conditions. The PDSI could describe drought events well because it is estimated through a water-balance model that accounts for temperature, precipitation and soil characteristic (Palmer, 1965; Dai *et al.*, 2004; Dai, 2011). The sc_PDSI was strongly and significantly negatively correlated with the tree-ring δ^{18}O in July and August, which reflects the comprehensive influence of the climatic factors embodied in sc_PDSI on tree-ring δ^{18}O. The sc_PDSI in July and August was the most meaningful single variable that explained the variation in our δ^{18}O chronology based on its climate response.

3.3. Calibration and verification

On the basis of tree-ring δ^{18}O-climate relationships described in Section 3.2, we used tree-ring δ^{18}O as independent variable and sc_PDSI in July–August as the dependent variable to establish a transfer function. The resulting reconstruction accounted for 38.4% (after adjusted the degree of freedom) of the total variance during the validation period from 1959 to 2008 (Figure 3(c)). The transfer function was significant ($F = 32.51$, $p < 0.001$). The residuals of the regression model showed normal distribution with a Shapiro–Wilk value of 0.98 ($p = 0.55$). Figure 3(d) showed that the residuals of the linear model did not vary with the tree-ring δ^{18}O values. This suggested that the residuals of the linear model had homogeneity of variance. The residuals had no significant trend with the predicted sc_PDSI (Figure 3(e)). The linear model had Durbin–Watson value of 1.55 and no significant autocorrelation was detected in the residual series. All of above suggested that the regression was valid to represent the relationship between the July–August sc_PDSI and the tree-ring δ^{18}O. The uncertainty of the reconstructed sc_PDSI arises mainly from uncertainty of the model and the δ^{18}O measurements (Figure 2). We estimated the uncertainty associated with the linear model using bootstrap method. A calibration set (2/3 of the data) was sampled with replacement, the best linear model was estimated on this data and the quality of the reconstruction was assessed by the rest of the data (verification sample). After 1000 iterations of this method, we estimated the uncertainty on the sc_PDSI as the mean standard deviations of the verification residuals (2.19). Then, the uncertainties of the δ^{18}O measurements were added through multiplication by the constant coefficient in the linear model.

The statistics of calibration and verification indicated that the model was applicable with positive RE and CE, and significant *r* and ST except for the verification period from 1948 to 1958 (Table 1). The insignificant verification statistics from 1948 to 1958 might arise from the degradation of the data of sc_PDSI due to the data interpolated from the near meteorological stations. The results of the leave-one-out method also demonstrated that the transfer function was valid, with a RE and CE both of 0.35, a correlation coefficient of 0.63 and a sign test of 40+/10− ($p < 0.01$). The reconstruction of the July–August sc_PDSI was consistent with the gridded values from 1959 to 2008 (Figure 3(f)). Results of the spatial correlation analysis showed that the reconstruction reflected a broad range of drought variability in the northwestern China, Western Mongolia and parts of central Asia. The strongest UCAR 1900–2008 correlations coincided with the study region. The pattern of the spatial correlation between reconstruction and UCAR sc_PDSI were similar for the two periods of from 1950 to 2008 and from 1900 to 2008, but the strength was stronger for the period of from 1950 to 2008 (Figure 4(a) and (b)). The spatial correlation pattern between reconstruction and SPEI was similar to the UCAR sc_PDSI (Figure 4(a) and (c)). These evidences further suggest that the reconstruction is robust, and agrees with reanalysis datasets (i.e. UCAR sc_PDSI and SPEI) that extend further back in time.

Table 1. Calibration/verification statistics for the reconstructed sc_PDSI in July and August; the calibration was performed over a 30-year interval. The results of the leave-one-out validation method.

	Calibration	*r*	ST	Verification	*r*	RE	CE	ST
	1959–1988	0.60**	23/7*	1989–2008	0.69**	0.41	0.43	17/3*
	1989–2008	0.69**	17/3*	1959–1988	0.60**	0.28	0.32	23/7*
	1979–2008	0.70**	24/6*	1959–1978	0.52**	0.19	0.15	16/4*
	1959–2008	0.63**	40/10**	1948–1958	0.06^{ns}	−0.65	−0.4	6/5^{ns}
Leave-one-out	1959–2008	0.63**	40/10**			0.35	0.35	

ns, not significant. *$p < 0.05$. **$p < 0.01$.

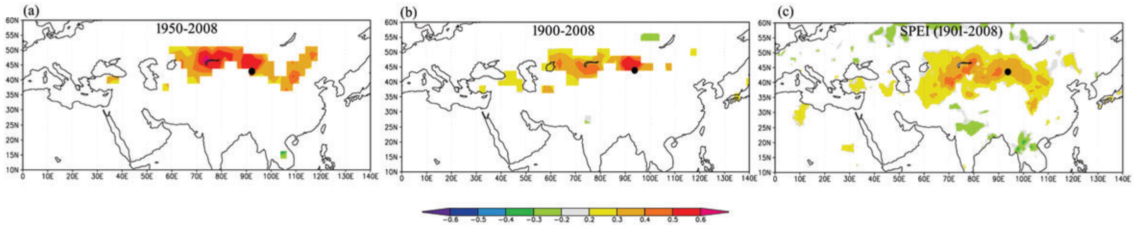

Figure 4. Spatial correlation ($p < 0.1$) pattern of the reconstruction with the sc_PDSI data from the regional grid (UCAR; Dai, 2011) from 1950 to 2008 (a) and from 1900 to 2008 (b); and (c) with the SPEI data (Vicente-Serrano *et al.*, 2010) from 1901 to 2008. The black dots represent sampling site. The analyses were accomplished using the KNMI Climate Explorer software (http://climexp.knmi.nl).

3.4. Reconstruction and validation of July–August sc_PDSI

The past 309-year July–August sc_PDSI were reconstructed by applying the transfer function. The regional moisture conditions became wetter from 1700 to 1850 (slope = 0.02, $R^2 = 0.13$, $p < 0.001$) and drier from 1993 to 2008 (slope = −0.25, $R^2 = 0.37$, $p = 0.008$; Figure 5(a)). We conducted a regime shift analysis to test the mean value shift of our reconstruction using software Regime Shift Detection v3.2 (Rodionov, 2006). We found six major regime shifts in years 1710, 1785, 1808, 1830, 1855, 1898 and 2006. During the 19th century, the sc_PDSI showed three regime shift periods, which indicated that the moisture conditions were not stable in this period. The dry period (with sc_PDSI relative lower values) occurred from 1700 to the 1780s, from the 1810s to the 1820s, from the 1850s to the 1890s and the 2000s. The wet periods (with sc_PDSI relative higher value) occurred from 1780 to the 1800s, from the 1830s to 1850 and the whole 20th century (Figure 5(a) and (b)). The extreme years are defined as those reconstructed residual sc_PDSI values exceeding 1.5 standard deviation from the base level (thick solid lines in Figure 5(a)). In total, there was 35 extreme years (accounted for 11.3% of total years) during the past 309 years. The extreme dry years (downward bars) were concentrated in the period from 1700 to 1730, whereas the extreme wet years (upward bars) were concentrated in the period from the 1740s to the 1770s and from the 1880s to the 1920s.

Several moisture-sensitive tree-ring records in the area surrounding our study area provide evidence to validate our sc_PDSI reconstruction (Figure 5). Our reconstruction showed a high correlation with the PDSI reconstruction in June–July–August (JJA) from the Monsoon Asia Drought Atlas (MADA) (Cook *et al.*, 2010) at the grid 220 (43.75°93.75°; Figures 1 and 5(c)) and grid 219 (41°25′N, 93.75°E; Figures 1 and 5(d)) with correlation coefficients of 0.26 and 0.28 ($p < 0.01$, $n = 306$) covering the common period from 1700 to 2005, respectively. These correlation coefficients reached to 0.65 and 0.56 during the instrumental period (1959–2005) for grid 220 and 219, respectively. But the correlation between our reconstruction and MADA PDSI was relatively low (0.40 and 0.55) during the period of 1900–1958, especially from 1920 to 1958 ($r = 0.08$ and $r = 0.23$, $p > 0.1$). This indicated that the coherence between reconstructed sc_PDSI and MADA PDSI was not strong during the early 20th century. The different signal window (i.e. JA *vs* JJA) and site-specific reconstruction may cause this discrepancy. During the past century (1900–2005), the correlation between this reconstruction and the MADA (Cook *et al.*, 2010) attained to 0.47 and 0.48 for grid 220 and 219, respectively. In addition, the dry periods occurred from 1707 to the 1730s, and during the 1850s, the 1930s and the 1970s. The wet periods occurred during the 1780s, the 1800s, from 1950 to the 1960s and from 1980 to the 1990s, which agree with the results of the MADA results. The wetter 20th century agreed with the results of MADA (Cook *et al.*, 2010) in the Miquan, the central Tianshan Mountain (Li *et al.*, 2006) (Figure 5(e)) and in northern Pakistan (Treydte *et al.*, 2006) (Figure 5(f)). The wet period from 1780 to 1800 also occurred in the Miquan results (Li *et al.*, 2006), a period that corresponds to a strong advance of the Glacier NO.1 in the source area of the Urumqi River, in the central of the Tianshan Mountains, around 1770 ± 20 years (Chen, 1989). The dry period from 1700 to 1780s was agreed with the less precipitation in northern Pakistan (Treydte *et al.*, 2006).

However, some discrepancies also existed among different reconstructions during several periods. The reconstructed sc_PDSI showed differing changes from MADA PDSI, Miquan PDSI and precipitation in northern Pakistan from 1750 to 1780. During the period of 1810–1870, sc_PDSI reconstruction was less coordinated with the Miquan PDSI and precipitation in northern Pakistan. The sc_PDSI reconstruction was different from the Miquan PDSI from 1950 to 2002, but showed similar fluctuations with MADA PDSI during this period. Our reconstruction showed no significant correlation with the patterns of PDSI in April to June from Miquan (Li *et al.*, 2006) and annual precipitation in northern Pakistan (Treydte *et al.*, 2006). The discrepancies may have resulted from the local setting and seasonal characteristics over the regions. The different signal window among the reconstruction may also cause the discrepancies. For example, the sc_PDSI reconstruction spanned from July to August, the MADA PDSI is from June to August, while the Miquan PDSI is from April to June.

The reconstruction showed a decreasing trend from the 1990s to 2008, which was similar to the result of MADA (Cook *et al.*, 2010). But this result differed from the result

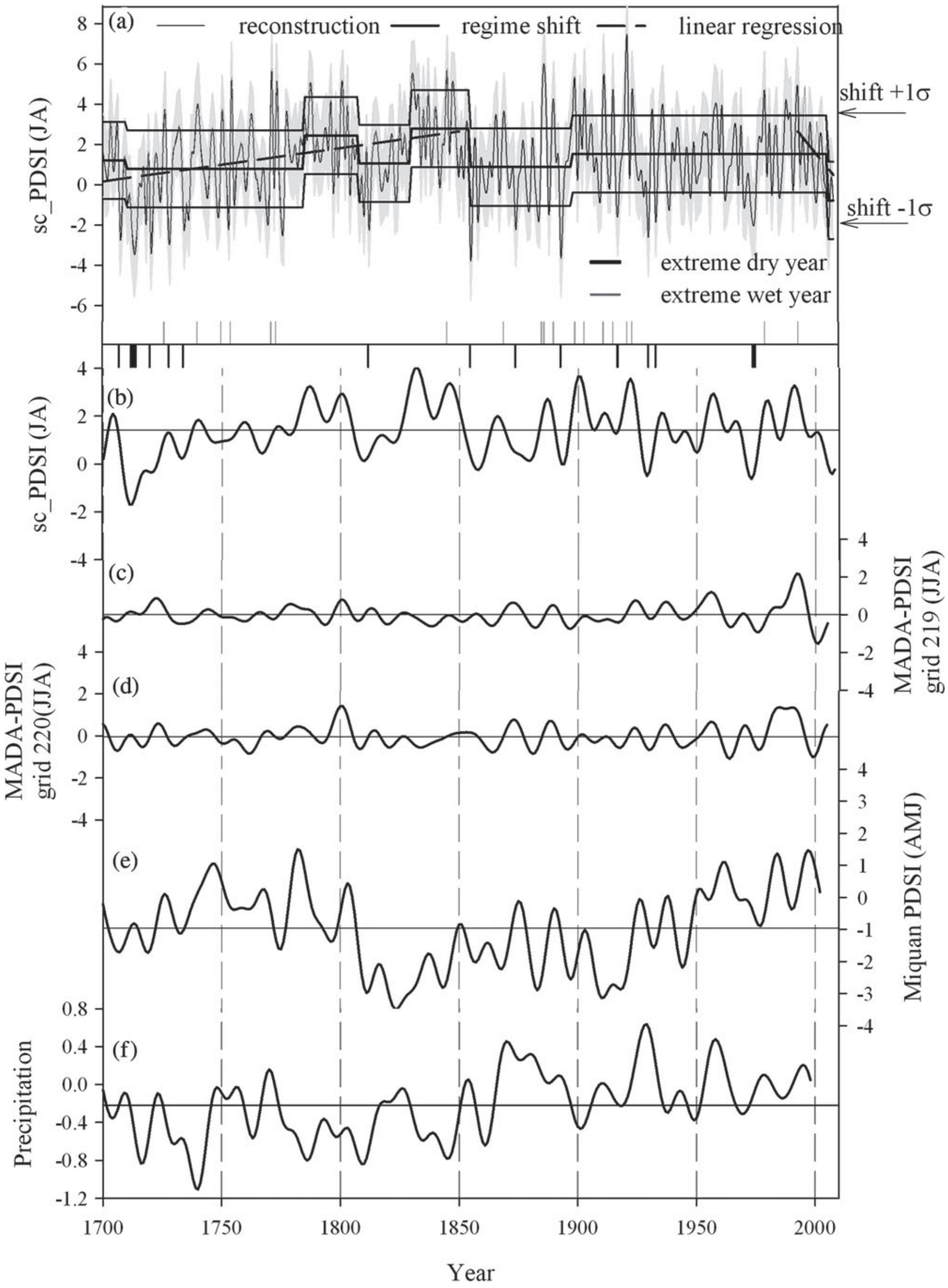

Figure 5. (a) Reconstructed July–August sc_PDSI with its regime shift. The black line is the reconstructed sc_PDSI, with its uncertainty showed in grey shading ($\pm 1\sigma$), the thick solid line is the regime shifts (cutoff length =10 years, confident at 95%); the thick dashed lines represent the regression of sc_PDSI with the time, respectively, during 1700–1850 and 1993–2008; the upward and downward bars corresponded to extreme wet/dry years (see text for details). Comparisons between (b) the present sc_PDSI reconstruction and (c, d) the gridded (ID 219 and ID 220) June to August (JJA) PDSI data from the MADA dataset (Cook *et al.*, 2010), (e) the April to June (AMJ) PDSI in Miquan (Li *et al.*, 2006); and (f) annual precipitation reconstruction in northern Pakistan (Treydte *et al.*, 2006). The central line represents the long-term mean value. (b–f) Smoothed results based on 10-year FFT.

of the Shi *et al.* (2007), who reported a warmer and wetter trend since 1987 in the northern part of Xinjiang region. Our results demonstrated that the moisture levels have not been increasing during last two decades in the eastern Tianshan Mountains, which is confirmed by the results of other studies (Ma *et al.*, 2005; Zou *et al.*, 2005). As moisture levels are regionally variable, representation of many regions is needed to understand hydroclimatic changes over long-time scales in China.

Over the long term, our sc_PDSI reconstruction captured more of the low-frequency of variations than in the MADA dataset (Cook *et al.*, 2010) before 1950 (Figure 5). One possible explanation arises from differences in the calibration approaches and instrumental ‘targets’ (Esper *et al.*, 2005). In the MADA reconstruction, the calibration period for PDSI values was from 1951 to 1989, and the verification period was from 1920 to 1950, and the series ended in 1989 (Cook *et al.*, 2010). Instrumental data from 1990 to 2005 were appended to the ends of the MADA datasets (NOAA Paleoclimatology, http://www.ncdc.noaa.gov/paleo). The sc_PDSI data before the instrument period were interpolated from meteorological records recorded in surrounding areas (Dai *et al.*, 2004; Dai, 2011). Thus, the quality of that data for northwestern China is degraded before the instrument period. Our reconstruction used these relatively precise data as calibrate data, and thereby obtained robust results in the reconstruction. In addition, the PDSI in MADA (Cook *et al.*, 2010) combined many remote datasets based on a large search radius (e.g. 1000 km) to locate the candidate tree-ring predictors, and thus lost some local information and bring some uncertainties. Our reconstruction contained more local drought information about period of less intense dryness or wetness at local scales. Similar discrepancies between the PDSI reconstruction from the MADA datasets and site-based reconstructions were also founded in northern China (Fang *et al.*, 2012). Last but not least, the influence of the detrending method used for the tree-ring width data may have caused some discrepancies. The standardization procedure that is used to remove any nonclimatic variability retained in the ring-width measurements often results in a loss of data on climate variations on centennial and longer time scales (Cook *et al.*, 1995), although this can be largely overcome by proper treatment using methods such as regional curve standardization by applying a large number of ring-width series (Esper *et al.*, 2002; Schweingruber, 2003). In contrast, tree-ring δ^{18}O series are not processed by data-adaptive curve fitting, and so there is no potential loss of low-frequency variability in δ^{18}O-based climate reconstructions.

3.5. Linkages to NAO and ENSO

Our reconstruction showed fluctuations similar to those of the July–August NAO index in most of the common periods with a weak correlation coefficient 0.15 ($p = 0.07$) from 1873 to 2008 (Figure 6(a) and (b)). That suggests that the NAO might influence moisture conditions in the eastern Tianshan Mountains in the long term. Changes in the NAO phase are associated with characteristic changes in surface temperature, precipitation and storm tracks over the Mediterranean Basin and Eurasia (Dickson *et al.*, 2000). In northwestern China, the atmospheric moisture flux is mainly transported by the westerly circulation (Feng *et al.*, 2004; Li *et al.*, 2008), and moist air in our study area mainly comes from the west, northwest and north (Dai *et al.*, 2006; Liu *et al.*, 2009b; Yang *et al.*, 2010). The NAO represents the strength of the westerly circulation (Hurrell *et al.*, 2001; Li and Wang, 2003; Pinto and Raible, 2012). When the NAO is in its positive phase, the water flux convergence in our study area is strong, resulting in increased water vapour concentrations and precipitation, whereas the negative phase of the NAO decreases water vapour and precipitation as a result of divergence of water flux (Li *et al.*, 2008). Other evidence suggested the existence of anomalous convergences in lower layers of the atmosphere and divergences in the upper layers of the atmosphere that correspond to an anomalous barotropical depression over central and eastern Asia and our study area during a summer when the NAO is in its positive phase (Sun and Wang, 2012). Therefore, the positive (negative) phase of the NAO corresponded to wetter (dry) regional moisture conditions. However, we also noted periods when the relationships

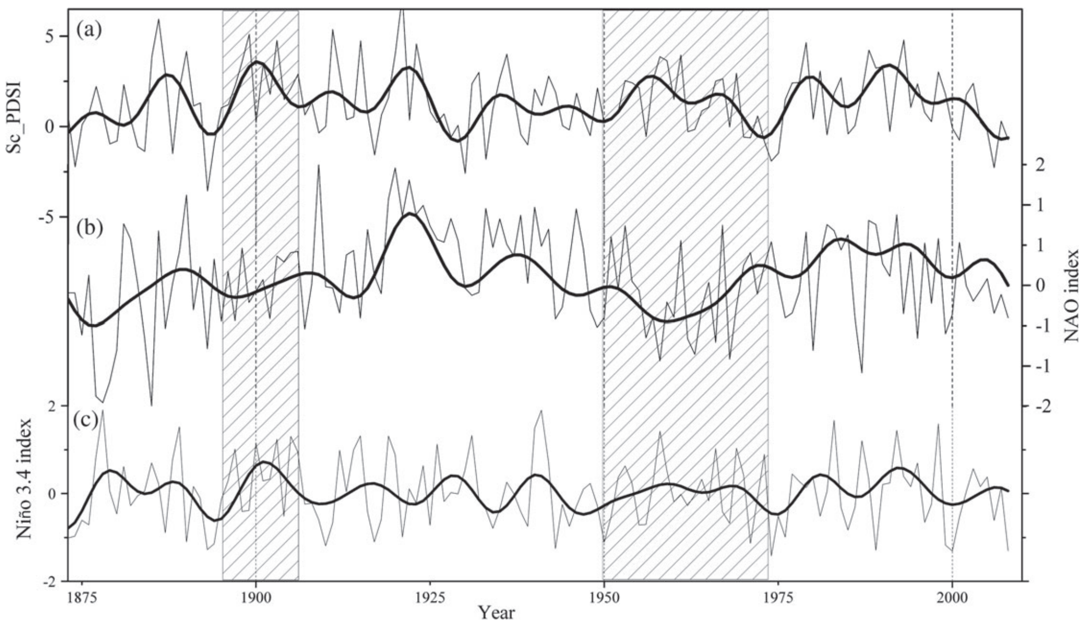

Figure 6. Comparisons between (a) our sc_PDSI reconstruction and (b) the NAO index in July–August (Li and Wang, 2003), and (c) the Niño 3.4 index data from January to April for 1856–2008 (Kaplan *et al.*, 1998; http://www.cpc.ncep.noaa.gov). In all graphs, we only showed the values during their common periods (1873–2008), and values (heavy lines) are the smoothed results based on a FFT band-pass filter to retain the signals at scales from 10 to 60 years. The two shaded periods (around the 1900s and from 1950 to 1975) represent times when the three series showed different trends.

between the NAO and sc_PDSI were disturbed, such as around 1890 to 1910 and 1950 to 1975, suggesting that other factors might affect the variation in moisture condition in our study area during certain periods.

The variations in NAO are associated with the ENSO (Melo-Gonçalves *et al.*, 2005). The NAO and ENSO phenomena both affect the precipitation in central and southwestern Asia (Syed *et al.*, 2006; 2010). In this study, the sc_PDSI reconstruction was weakly but significantly correlated ($r = 0.31$, $p = 0.0002$, $n = 136$) with the Niño 3.4 index from January to April for the period from 1856 to 2008. The sc_PDSI reconstruction follows the Nino 3.4 index at both annual and longer scales (Figure 6(a) and (c)). These results suggest that ENSO might also affect the moisture conditions in the study area. Similar results have also been reported for the correlation with tree-ring width index from the middle of the Tianshan Mountains (Li *et al.*, 2010).

On the basis of precipitation data in the northern Xinjiang region, several studies have found that during the warm phase of ENSO, El Niño, the 4-month-lagged precipitation was greater than that in normal years, whereas precipitation was lower during the cold phase, La Niña (Li, 1989; Ren, 1989; Zhang and Chen, 2001). The relationship between sc_PDSI reconstruction and ENSO is in good agreement with recent studies that have suggested that the drought in central and southwestern Asia results from the cold phase of ENSO in the tropical oceans (Barlow *et al.*, 2002; Hoerling and Kumar, 2003). Climate models have consistently demonstrated that drying over central Asia is linked with temperature variations in the oceans (Hoerling and Kumar, 2003; Mariotti, 2007). The interaction between the tropical and mid-latitude climates occurs when the warmer ENSO phase induces an anomalous southwesterly moisture flux (Mariotti, 2007). The increased southwesterly moisture flux brings abundant moisture into central and southwestern Asia, causing increased precipitation (Zhao *et al.*, 2006; Mariotti, 2007). During the ENSO cold phase, southwesterly moisture flux decreases, leading to decreased transfer of moisture into central and southwestern Asian, leading to drought (Hoerling and Kumar, 2003; Mariotti, 2007). Our result revealed that the linkages between drought and ENSO were relatively stable in the long term.

The NAO and Niño3.4 index after band-pass filter could explain 17.6% ($r = 0.42$, $p < 0.01$) of the total variations of sc_PDSI by multiple regression analysis. This may suggest that synergy of the NAO and ENSO affects the regional drought at the decadal scales. The ENSO sea surface temperature affects the variation in NAO (Melo-Gonçalves *et al.*, 2005), and the interaction between the two phenomena can therefore influence the frequency and severity of drought in our study area (Hoerling and Kumar, 2003). These linkages could explain the relationships among the sc_PDSI reconstruction, the NAO index and ENSO around the 1900s and from 1950 to 1975. However, the relationships between the NAO internal variability and ENSO in different period should be further explored by the atmospheric modelling.

4. Conclusion

The availability of moisture is the primary factor that controls tree-ring δ^{18}O in the east Tianshan Mountains of northwestern China, which is indicated by significant positive correlations between tree-ring δ^{18}O and temperature (maximum and mean) and significant negative correlations with precipitation and relative humidity. Sc_PDSI values in July–August, which integrate these effects, were significantly negatively correlated with the tree-ring δ^{18}O, and we were able to establish a linear regression model that could reconstruct the July–August sc_PDSI series. The reconstruction showed similar trends to those in the MADA PDSI dataset, but revealed profound information on low-frequency variations in the local moisture conditions, suggesting the need to develop more drought reconstructions with different proxy parameters. Our reconstruction showed wet epochs from 1780 to the 1800s, from the 1830s to 1850 and during the 20th century. Dry periods occurred from 1700 to the 1780s, from the 1810s to the 1820s, from the1850s to the 1890s and the 2000s. The variation in drought intensity was likely linked with the NAO, but the relationship was also disturbed by ENSO around the 1900s and from 1950 to 1975.

Acknowledgements

We are grateful for the editors and reviewers for valuable comments and suggestions that substantially improved the manuscript. This research was supported by the Global Change Research Program of China (2010CB951401), by the National Natural Science Foundation of China (41171167 and 31200299), by the China Desert Meteorological Science Research Foundation (Sqj2011013 and Sqj2009001), by Project for Incubation of Specialists in Glaciology and Geocryology of National Natural Science Foundation of China (J0930003/J0109), by a Chinese Academy of Sciences Special Grant for Postgraduate Research, Innovation and Practice and by the Chinese Academy of Sciences Interdisciplinary Innovation Team project (29Y329B91). We thank Prof. Xiaohua Gou for providing Miquan PDSI data used in our comparison.

References

Abaimov AP. 2010. Geographical distribution and genetics of Siberian larch species. In *Permafrost Ecosystems*, Osawa A, Zyryanova OA, Matsuura Y, Kajimoto T, Wein RW. (eds). Springer: Dordrecht, Netherlands; 41–58.

Anchukaitis KJ, Evans MN. 2010. Tropical cloud forest climate variability and the demise of the Monteverde golden toad. *Proc. Natl. Acad. Sci.* **107**: 5036–5040, DOI: 10.1073/pnas.0908572107.

Barlow M, Cullen H, Lyon B. 2002. Drought in central and southwest Asia: La Niña, the warm pool, and Indian Ocean precipitation. *J. Clim.* **15**: 697–700.

Bergland G. 1969. A guided tour of the fast Fourier transform. *IEEE Spectr.* **6**: 41–52.

Chen JY. 1989. Preliminary studies on using lichen dating to study Holocene glacial changes in the source region of Urumqi River, Tianshan. *Sci. China, Ser. B* **32**: 1487–1500.

Cook ER, Kairiukstis LA. 1990. *Methods of Dendrochronology: Applications in the Environmental Sciences*. Kluwer Academic Publishers: Boston, MA.

Cook ER, Briffa KR, Meko DM, Graybill DA, Funkhouser G. 1995. The 'segment length curse in' long tree-ring chronology development for palaeoclimatic studies. *The Holocene* **5**: 229–237.

Cook ER, Anchukaitis KJ, Buckley BM, D'Arrigo RD, Jacoby GC, Wright WE. 2010. Asian monsoon failure and megadrought during the Last millennium. *Science* **328**: 486–489, DOI: 10.1126/science.1185188.

Dai A. 2011. Characteristics and trends in various forms of the Palmer Drought Severity Index during 1900–2008. *J. Geophys. Res.* **116**: D12115, DOI: 10.1029/2010JD015541.

Dai A, Trenberth KE, Qian T. 2004. A global dataset of palmer drought severity index for 1870–2002: relationship with soil moisture and effects of surface warming. *J. Hydrometeorol.* **5**: 1117–1130, DOI: 10.1175/JHM-386.1.

Dai XG, Li WJ, Ma ZG. 2006. Variation characteristics of moisture source of Xinjiang, China in recent decades (in Chinese). *Prog. Nat. Sci.* **16**(12): 1651–1656.

Dansgaard W. 1964. Stable isotopes in precipitation. *Tellus* **16**: 436–468.

Daux V, Edouard JL, Masson-Delmotte V, Stievenard M, Hoffmann G, Pierre M, Mestre O, Danis PA, Guibal F. 2011. Can climate variations be inferred from tree-ring parameters and stable isotopes from *Larix decidua*? Juvenile effects, budmoth outbreaks, and divergence issue. *Earth Planet. Sci. Lett.* **309**: 221–233, DOI: 10.1016/j.epsl.2011.07.003.

Davison AC, Hinkley DV. 1997. *Bootstrap Methods and Their Application. Cambridge Series in Statistical and Probabilistic Mathematics*. Cambridge University Press: Cambridge, UK.

Dickson R, Osborn T, Hurrell J, Meincke J, Blindheim J, Adlandsvik B, Vinje T, Alekseev G, Maslowski W. 2000. The Arctic Ocean response to the North Atlantic Oscillation. *J. Clim.* **13**: 2671–2696.

Easterling D, Evans J, Groisman PY, Karl T, Kunkel K, Ambenje P. 2000. Observed variability and trends in extreme climate events: a brief review. *Bull. Am. Meteorol. Soc.* **81**: 417–426.

Esper J, Cook ER, Schweingruber FH. 2002. Low-frequency signals in long tree-ring chronologies for reconstructing past temperature variability. *Science* **295**: 2250–2253.

Esper J, Frank DC, Wilson RJ, Briffa KR. 2005. Effect of scaling and regression on reconstructed temperature amplitude for the past millennium. *Geophys. Res. Lett.* **32**: L07711, DOI: 10.1029/2004GL021236.

Esper J, Frank DC, Battipaglia G, Büntgen U, Holert C, Treydte K, Siegwolf R, Saurer M. 2010. Low-frequency noise in δ^{13}C and δ^{18}O tree ring data: a case study of Pinus uncinata in the Spanish Pyrenees. *Glob. Biogeochem. Cycles* **24**: GB4018, DOI: 10.1029/2010gb003772.

Fang KY, Gou XH, Chen FH, Liu CZ, Davi N, Li JB, Zhao ZQ, Li YJ. 2012. Tree-ring based reconstruction of drought variability (1615–2009) in the Kongtong Mountain area, northern China. *Glob. Planet. Change* **80–81**: 190–197, DOI: 10.1016/j.gloplacha.2011.10.009.

Feng W, Wang KL, Jiang H. 2004. Influences of westerly wind interannual change on water vapor transport over northwest China summer (in Chinese). *Plateau Meteorol.* **23**(02): 271–275.

Fritts HC. 1976. *Tree Rings and Climate*. Academic Press: London, UK.

Hoerling M, Kumar A. 2003. The perfect ocean for drought. *Science* **299**: 691–694.

Holmes RL. 1983. Computer-assisted quality control in tree-ring dating and measurement. *Tree-Ring Bull.* **43**: 69–78.

Hurrell JW, Kushnir Y, Visbeck M. 2001. The North Atlantic Oscillation. *Science* **291**: 603–605.

Kaplan A, Cane M, Kushnir Y, Clement A, Blumenthal M, Rajagopalan B. 1998. Analyses of global sea surface temperature 1856–1991. *J. Geophys. Res.* **103**: 567–589.

Kress A, Saurer M, Siegwolf RTW, Frank DC, Esper J, Bugmann H. 2010. A 350 year drought reconstruction from Alpine tree ring stable isotopes. *Glob. Biogeochem. Cycles* **24**: GB2011, DOI: 10.1029/2009gb003613.

Laumer W, Andreu L, Helle G, Schleser GH, Wieloch T, Wissel H. 2009. A novel approach for the homogenization of cellulose to use micro-amounts for stable isotope analyses. *Rapid Commun. Mass Spectrom.* **23**: 1934–1940, DOI: 10.1002/rcm.4105.

Leavitt SW. 2008. Tree-ring isotopic pooling without regard to mass: no difference from averaging δ^{13}C values of each tree. *Chem. Geol.* **252**: 52–55, DOI: 10.1016/j.chemgeo.2008.01.014.

Leavitt SW. 2010. Tree-ring C-H-O isotope variability and sampling. *Sci. Total Environ.* **408**: 5244–5253, DOI: 10.1016/j.scitotenv.2010.07.057.

Li DC. 1989. Relationships between El Niño and the temperature and precipitation in northwestern Xinjiang (in Chinese). *Xinjiang Meteorol.* **Z2**: 1–5.

Li JP, Wang JXL. 2003. A new North Atlantic Oscillation index and its variability. *Adv. Atmos. Sci.* **20**: 661–676.

Li JB, Gou X, Cook ER, Chen F. 2006. Tree-ring based drought reconstruction for the central Tien Shan area in northwest China. *Geophys. Res. Lett.* **33**: L07715, DOI: 10.1029/2006gl025803.

Li WL, Wang KL, Fu SM, Jiang H. 2008. The interrelationship between regional westerly index and the water vapor budget in Northwest China (in Chinese). *J. Glaciol. Geocryol.* **30**: 28–34.

Li JB, Cook ER, Chen F, Gou X, D'Arrigo R, Yuan Y. 2010. An extreme drought event in the central Tien Shan area in the year 1945. *J. Arid Environ.* **74**: 1225–1231.

Liñán ID, Gutiérrez E, Helle G, Heinrich I, Andreu-Hayles L, Planells O, Leuenberger M, Burger C, Schleser G. 2011. Pooled versus separate measurements of tree-ring stable isotopes. *Sci. Total Environ.* **409**: 2244–2251, DOI: 10.1016/j.scitotenv.2011.02.010.

Liu JR, Song X, Sun X, Yuan G, Liu X, Wang S. 2009a. Isotopic composition of precipitation over Arid Northwestern China and its implications for the water vapor origin. *J. Geogr. Sci.* **19**: 164–174, DOI: 10.1007/s11442-009-0164-3.

Liu X, Shao X, Liang E, Chen T, Qin D, An W, Xu G, Sun W, Wang Y. 2009b. Climatic significance of tree-ring δ^{18}O in the Qilian Mountains, northwestern China and its relationship to atmospheric circulation patterns. *Chem. Geol.* **268**: 147–154, DOI: 10.1016/j.chemgeo.2009.08.005.

Liu XH, Liu Y, Xu GB, Cai QF, An WL, Wang WZ. 2010. Pretreatment of the tree-ring samples for stable isotope analysis (in Chinese). *J. Glaciol. Geocryol.* **32**: 1242–1250.

Liu X, An W, Treydte K, Shao X, Leavitt S, Hou S, Chen T, Sun W, Qin D. 2012. Tree-ring δ^{18}O in southwestern China linked to variations in regional cloud cover and tropical sea surface temperature. *Chem. Geol.* **291**: 104–115, DOI: 10.1016/j.chemgeo.2011.10.001.

Loader NJ, Robertson I, Switsur VR, Waterhouse JS. 1997. An improved technique for the batch processing of small whole wood samples to α-cellulose. *Chem. Geol.* **136**: 313–317.

Ma Z, Fu C. 2006. Some evidence of drying trend over northern China from 1951 to 2004. *Chin. Sci. Bull.* **51**: 2913–2925.

Ma Z, Huang G, Gan W, Chen L. 2005. Multi scale temporal characteristics of the dryness/wetness over Northern China during the last century (in Chinese). *Chin. J. Atmos. Sci.* **29**: 678–681.

Mariotti A. 2007. How ENSO impacts precipitation in southwest central Asia. *Geophys. Res. Lett.* **34**: L16706, DOI: 10.1029/2007GL030078.

McCarroll D, Loader NJ. 2004. Stable isotopes in tree rings. *Quat. Sci. Rev.* **23**: 771–801, DOI: 10.1016/j.quascirev.2003.06.017.

Melo-Gonçalves P, Rocha A, Castanheira J, Ferreira J. 2005. North Atlantic Oscillation sensitivity to the El Niño/Southern Oscillation polarity in a large-ensemble simulation. *Clim. Dyn.* **24**: 599–606, DOI: 10.1007/s00382-005-0001-z.

Palmer WC. 1965. Meteorological Drought. US Department of Commerce, Weather Bureau: Washington, D.C.

Pinto JG, Raible CC. 2012. Past and recent changes in the North Atlantic oscillation. *Wiley Interdiscip. Rev.: Clim.Change* **3**: 79–90, DOI: 10.1002/wcc.150.

Porter TJ, Middlestead P. 2012. On estimating the precision of stable isotope ratios in processed tree-rings. *Dendrochronologia* **30**: 239–242, DOI: 10.1016/j.dendro.2012.02.001.

Porter TJ, Pisaric MF, Field RD, Kokelj SV, Edwards TW, Healy R, LeGrande AN. 2013. Spring-summer temperatures since AD 1780 reconstructed from stable oxygen isotope ratios in white spruce tree-rings from the Mackenzie Delta, northwestern Canada. *Clim. Dyn.* **1–15**, DOI: 10.1007/s00382-013-1674-3.

Rashed M, Li S, Babar K. 2010. Causes of recurring drought patterns in Xinjiang, China. *J. Arid Land* **2**: 279–285, DOI: 10.3724/SP.J.1227.2010.00279.

Ren YY. 1989. The relationship between ENSO and Xinjiang weather (in Chinese). *Xinjiang Meteorol.* **12**: 6–10.

Rinn F. 2003. *TSAPWin: Time Series Analysis and Presentation for Dendrochronology and Related Applications*. Version 0.55 User Reference: Heidelberg, Germany.

Robertson I, Waterhouse JS, Barker AC, Carter AHC, Switsur VR. 2001. Oxygen isotope ratios of oak in east England: implications for reconstructing the isotopic composition of precipitation. *Earth Planet. Sci. Lett.* **191**: 21–31.

Roden JS, Ehleringer JR. 2000. Hydrogen and oxygen isotope ratios of tree ring cellulose for field-grown riparian trees. *Oecologia* **123**: 481–489.

Roden JS, Lin G, Ehleringer JR. 2000. A mechanistic model for interpretation of hydrogen and oxygen isotope ratios in tree-ring cellulose. *Geochim. Cosmochim. Acta* **64**: 21–35.

Rodionov SN. 2006. The problem of red noise in climate regime shift detection. *Geophys. Res. Lett.* **31**: L12707, DOI: 10.1029/2004GL019448.

Sano M, Ramesh R, Sheshshayee M, Sukumar R. 2012a. Increasing aridity over the past 223 years in the Nepal Himalaya inferred from a tree-ring δ^{18}O chronology. *The Holocene* **22**: 809–817, DOI: 10.1177/0959683611430338.

Sano M, Xu C, Nakatsuka T. 2012b. A 300-year Vietnam hydroclimate and ENSO variability record reconstructed from tree ring δ^{18}O. *J. Geophys. Res.* **117**: D12115, DOI: 10.1029/2012JD017749.

Saurer M, Schweingruber F, Vaganov EA, Shiyatov SG, Siegwolf R. 2002. Spatial and temporal oxygen isotope trends at the northern tree-line in Eurasia. *Geophys. Res. Lett.* **29**: 1296, DOI: 10.1029/2001gl013739.

Schweingruber FH. 2003. Tests of the RCS method for preserving low-frequency variability in long tree-ring chronologies. *Tree-Ring Res.* **59**: 81–98.

Shi Y, Shen Y, Kang E, Li D, Ding Y, Zhang G, Hu R. 2007. Recent and future climate change in northwest China. *Clim. Change* **80**: 379–393, DOI: 10.1007/s10584-006-9121-7.

Shi C, Masson-Delmotte V, Risi C, Eglin T, Stievenard M, Pierre M, Wang X, Gao J, Bréon F-M, Zhang Q-B, Daux V. 2011. Sampling strategy and climatic implications of tree-ring stable isotopes on the southeast Tibetan Plateau. *Earth Planet. Sci. Lett.* **301**: 307–316, DOI: 10.1016/j.epsl.2010.11.014.

Sternberg LSL. 2009. Oxygen stable isotope ratios of tree-ring cellulose: the next phase of understanding. *New Phytol.* **181**: 553–562, DOI: 10.1111/j.1469-8137.2008.02661.x.

Stokes MA, Smiley TL. 1968. *An Introduction of Tree-ring Dating*. The University of Chicago Press: Chicago, IL; 1–61.

Sun J, Wang H. 2012. Changes of the connection between the summer North Atlantic Oscillation and the East Asian summer rainfall. *J. Geophys. Res.* **117**: D08110, DOI: 10.1029/2012jd017482.

Syed F, Giorgi F, Pal J, King M. 2006. Effect of remote forcings on the winter precipitation of central southwest Asia part 1: observations. *Theor. Appl. Climatol.* **86**: 147–160, DOI: 10.1007/s00704-005-0217-1.

Syed FS, Giorgi F, Pal J, Keay K. 2010. Regional climate model simulation of winter climate over Central–Southwest Asia, with emphasis on NAO and ENSO effects. *Int. J. Climatol.* **30**: 220–235, DOI: 10.1002/joc.1887.

Szymczak S, Joachimski M, Bräuning A, Hetzer T, Kuhlemann J. 2012. Are pooled tree ring δ^{13}C and δ^{18}O series reliable climate archives?-a case study of *Pinus nigra* spp. *laricio* (Corsica/France). *Chem. Geol.* **308–309**: 40–49.

Tian L, Yao T, MacClune K, White JWC, Schilla A, Vaughn B, Vachon R, Ichiyanagi K. 2007. Stable isotopic variations in west China: a consideration of moisture sources. *J. Geophys. Res.* **112**: D10112, DOI: 10.1029/2006jd007718.

Treydte KS, Schleser GH, Helle G, Frank DC, Winiger M, Haug GH, Esper J. 2006. The twentieth century was the wettest period in northern Pakistan over the past millennium. *Nature* **440**: 1179–1182, DOI: 10.1038/nature04743.

Treydte K, Frank D, Esper J, Andreu L, Bednarz Z, Berninger F, Boettger T, D'Alessandro CM, Etien N, Filot M, Grabner M, Guillemin MT, Gutierrez E, Haupt M, Helle G, Hilasvuori E, Jungner H, Kalela-Brundin M, Krapiec M, Leuenberger M, Loader NJ, Masson-Delmotte V, Pazdur A, Pawelczyk S, Pierre M, Planells O, Pukiene R, Reynolds-Henne CE, Rinne KT, Saracino A, Saurer M, Sonninen E, Stievenard M, Switsur VR, Szczepanek M, Szychowska-Krapiec E, Todaro L, Waterhouse JS, Weigl M, Schleser GH. 2007. Signal strength and climate calibration of a European tree-ring isotope network. *Geophys. Res. Lett.* **34**: L24302, DOI: 10.1029/2007gl031106.

Vicente-Serrano SM, Beguería S, López-Moreno JI. 2010. A multiscalar drought index sensitive to global warming: the standardized precipitation evapotranspiration index. *J. Clim.* **23**: 1696–1718, DOI: 10.1175/2009jcli2909.1.

Waterhouse JS, Switsur VR, Barker AC, Carter AHC, Robertson I. 2002. Oxygen and hydrogen isotope ratios in tree rings: how well do models predict observed values? *Earth Planet. Sci. Lett.* **201**: 421–430.

Wells N, Goddard S, Hayes MJ. 2004. A self-calibrating Palmer drought severity index. *J. Clim.* **17**: 2335–2351.

Wigley T, Briffa K, Jones P. 1984. On the average value of correlated time series, with applications in dendroclimatology and hydrometeorology. *J. Clim. Appl. Meteorol.* **23**: 201–213.

Xu C, Sano M, Nakatsuka T. 2011. Tree ring cellulose δ^{18}O of *Fokienia hodginsii* in northern Laos: a promising proxy to reconstruct ENSO? *J. Geophys. Res.* **116**: D24109.

Yang Y, Chen Y, Li W, Wang M, Sun G. 2010. Impacts of climatic change on river runoff in northern Xinjiang of China over last fifty years. *Chin. Geogr. Sci.* **20**: 193–201, DOI: 10.1007/s11769-010-0193-y.

Yeh SW, Kug JS, Dewitte B, Kwon MH, Kirtman BP, Jin FF. 2009. El Niño in a changing climate. *Nature* **461**: 511–514, DOI: 10.1038/nature08316.

Young GHF, Demmler JC, Gunnarson BE, Kirchhefer AJ, Loader NJ, McCarroll D. 2011. Age trends in tree ring growth and isotopic archives: a case study of *Pinus sylvestris* L. from northwestern Norway. *Glob. Biogeochem. Cycles* **25**: GB2020, DOI: 10.1029/2010gb003913.

Zhang JB, Chen XM. 2001. Review the research of short-term climatic prediction in Xinjiang (in Chinese). *Xinjiang Meteorol.* **24**(5): 1–6.

Zhao BK, Cai CX, Yang LM, Wang H. 2006. Atmospheric circulation anomalies during wetting summer over Xinjiang region (in Chinese). *J. Glaciol. Geocryol.* **28**(3): 434–442.

Zhou WS, Li JF, Zhang JB. 1989. Some problems in developing the tree-ring chronologies in the south slope of the Altay mountain. In *Study of Tree-ring Climatology and Tree-ring Hydrology in Xinjiang*, Li JF, Zhang ZJ, Yuan YJ (eds). Meteorological Press: Beijing, China; 9–17.

Zou X, Zhai P, Zhang Q. 2005. Variations in droughts over China: 1951–2003. *Geophys. Res. Lett.* **32**: L04707, DOI: 10.1029/2004GL021853.

